Journal of Power Sources 252 (2014) 156–163

Contents lists available at ScienceDirect

Journal of Power Sources

journal homepage: www.elsevier.com/locate/jpowsour

# Platinum catalysts promoted by In doped $SnO_2$ support for methanol electrooxidation in alkaline electrolyte

Yuan-Yuan Feng*, Wei-Qing Kong, Qian-Ying Yin, Li-Xia Du, Ying-Ting Zheng, De-Sheng Kong

*Key Laboratory of Life-Organic Analysis, College of Chemistry and Chemical Engineering, Qufu Normal University, Qufu Shandong 273165, China*

## HIGHLIGHTS

- Composite metal oxides $In_xSnO_2$ are prepared with a simple hydrothermal process.
- $In_xSnO_2$ is used as functionalized support of Pt catalyst toward MOR.
- A small amount of In doped in $SnO_2$ exhibits much higher promoting effect to Pt.
- The increase in activity arises from the changes in the Pt electronic structure.

## ARTICLE INFO

*Article history:*
Received 7 September 2013
Received in revised form
22 November 2013
Accepted 2 December 2013
Available online 11 December 2013

*Keywords:*
Indium
Tin
Oxide
Platinum
Methanol electro-oxidation

## ABSTRACT

Composite metal oxides $In_xSnO_2$ are prepared with a simple hydrothermal process and used as functionalized support of Pt catalyst toward methanol electrooxidation reaction (MOR). The catalytic activity of Pt is strongly dependent on the composition of the support. Introduction of a small amount of In into $SnO_2$ support exhibits much higher promoting effect to the Pt catalytic properties as compared with Pt/$SnO_2$ and commercial Pt/C catalysts. The mass-specific activity (MSA) and intrinsic activity (IA) of Pt in Pt/$In_{0.1}SnO_2$ is 3.0 and 4.3 times that of Pt/C, respectively. Changes in Pt electronic structure arising from the interaction between Pt and the support are responsible for this improvement. Our findings clearly suggest that the composite metal oxides $In_xSnO_2$ can not only act as the catalyst support but also act as an effective promoter to Pt toward MOR, which would be promising in designing new catalysts that can replace the traditional catalytic nanostructure.



## 1. Introduction

Direct methanol fuel cells (DMFCs) are one of the very promising power sources for portable electronic devices and vehicles. It has been reported that the kinetics of both methanol anodic oxidation and oxygen cathodic reduction in alkaline electrolyte are more facile than in acidic electrolyte [1,2]. In addition, the electrode materials show much higher stability in alkaline electrolyte in comparison with that in acidic media. The above advantages make the alkaline direct methanol fuel cells exhibit a growing interest in recent years. To date, Pt is the most active catalyst toward methanol electro-oxidation reaction (MOR), nevertheless, it is easily poisoned by the CO-like intermediates formed in the MOR process, which strongly depresses the catalytic properties of Pt [3].

Recently, many researches focused on introducing a second metal into Pt to form bimetallic PtM catalysts (PtNi, PtRu, PtAu, PtAg, etc.) or Pt-on-M nanostructures (Pt-on-Ru, Pt-on-Co, etc.) [4–11] so as to improve the poison tolerance of Pt. The enhanced catalytic activity of Pt comes from the ligand effect [4,8–11] or bifunctional mechanism [5–7]. The ligand effect arises from the presence of other metals which change the electronic environment of Pt, giving rise to the modifications of the Pt electronic structure and consequently, the catalytic performance. The d-band center theory proposed by Nørskov and co-workers has been widely accepted and regarded as an indicator to determine the surface reactivity of Pt [12]. A downshift of d-band center would weaken the interaction between Pt and some simple adsorbates such as H, O, CO and thus improve the poison tolerance of Pt in the bimetallic PtM or Pt-on-M catalysts as compared with

* Corresponding author. Tel./fax: +86 537 4458301.
*E-mail address:* yfeng@mail.tsinghua.edu.cn (Y.-Y. Feng).

0378-7753/$ – see front matter © 2013 Elsevier B.V. All rights reserved.
http://dx.doi.org/10.1016/j.jpowsour.2013.12.008

pure Pt [12,13]. Difference in the work function between pure Pt and the Pt-based catalysts may play an important role for this improvement [14]. In addition, the promoter M can activate water at lower potentials than Pt, the adsorbed OH species on M can oxidize the −CO adsorbed on the surface of the neighboring Pt atoms to $CO_2$ and thus increase the CO tolerance of Pt [15], which is usually called synergistic effect or bifunctional mechanism. Besides the metal promoter, some metal oxides such as $CeO_2$, NiO and $V_2O_5$ are also investigated as the promoter to Pt toward MOR in alkaline electrolyte [16–21]. Shen et al. have reported that the addition of $CeO_2$ into Pt catalysts could significantly improve the catalytic activity and poisoning resistance of Pt toward alcohol electrooxidation due to the synergistic effect [19–21].

Supported catalysts are of special interest, for they allow for the fine dispersion and stabilization of small metal nanoparticles (NPs). Traditional DMFC catalysts use carbon material as the support because it has sufficient electronic conductivity, large surface area (e.g. 250 $m^2\ g^{-1}$ for XC-72 carbon black) and well-developed pore structure. The carbon materials can not only make the charge transport to/from the catalyst easily but also exhibit a high dispersion state of Pt on their surface [22]. However, during the repeated power-on and -off processes of fuel cells, the high potential often accelerates the carbon corrosion, which would make the Pt metal NPs be prone to agglomerating and thus lead to a decrease in their electrochemically active surface area (EAS) and activity [23,24]. In order to solve these problems, other support materials such as metal oxides are investigated [23,25–28]. It has been reported that the $TiO_2$-supported Pt catalyst show ultrahigh stability as compared with carbon-supported catalyst [23]. The $NbRu_yO_z$-supported Pt catalyst can facilitate the C–C scission and exhibit a much higher catalytic performance toward ethanol oxidation [26]. Recently, a nanostructured $Ti_{0.7}Mo_{0.3}O_2$ material was prepared and used as the support for Pt catalyst [27], the electron transferring from $Ti_{0.7}Mo_{0.3}O_2$ to Pt induces changes in the surface electronic structure of Pt, the catalytic activity of Pt toward oxygen reduction reaction (ORR) is then improved remarkably.

Although some metal oxides have been identified as good promoters to Pt, a small fraction of them can be used as catalyst support because of their poor electrical conductivity. Tin dioxide is electrically conductive, and the Pt or Pd-based electrocatalysts that are promoted by $SnO_x$ have shown high catalytic properties for the electrooxidation of small organic molecules due to the high CO-poisoning tolerance [29,30]. In addition, Sn-containing multicomponent metal oxides such as In-doped $SnO_2$ or Sn-doped $In_2O_3$ (ITO) have been used as a perfect conductive material in many fields, such as the liquid crystal displays, touch panels, plastic electroluminescent lamp and catalyst supports [31–33]. Inspired by the high electrical conductivity of ITO and the good promoting effect of $SnO_x$ to Pt toward the electrooxidation of small organic molecules [29], in the present work, we prepared the In-doped $SnO_2$ material through a traditional hydrothermal method. The multicomponent metal oxide materials are used as the catalyst support to carry Pt NPs toward the MOR in alkaline electrolyte. The promoting effect of the multicomponent In-doped $SnO_2$ materials arises from the ligand effects, which are related to the modification of the electronic structure of Pt [34] and vital for the enhancement of the Pt catalytic properties. Compared with the conventional carbon-supported Pt catalyst, small amount of In doping in $SnO_2$ support show much higher promoting effect to Pt catalytic activity and stability for MOR. These results are of fundamental importance to the in-depth understanding or the MOR mechanism and also exhibit potential applications in the design of fuel cell catalysts.

## 2. Experimental section

### 2.1. Synthesis of the $In_xSnO_2$ metal oxide supports

Traditional hydrothermal method was used to prepare the $In_xSnO_2$ nanostructures. Take the $In_{0.1}SnO_2$ for example: 2 mL $InCl_3$ (50 mM) and 20 mL $SnCl_4$ (50 mM) solution was stirred for 30 min and then transferred into a Teflon-lined autoclave with a stainless steel shell and heated to 200 °C in the oven. The sample was kept at 200 °C for 3 h and then cooled to room temperature. The as-prepared sample was washed with deionized water and centrifugated for several times. The precipitates were dried at 80 °C oven overnight. The $In_{0.8}SnO_2$ and $SnO_2$ samples were prepared through the same method only the ratio of the added metal precursors was different.

### 2.2. Preparation of the $In_xSnO_2$-supported Pt samples ($Pt/In_xSnO_2$)

Platinum NPs were prepared through the polyols method. 0.65 mL $H_2PtCl_4$ (0.04 M) and 20 mg sodium citrate were added into 15 mL ethylene glycol. After stirring for 30 min, sodium hydroxide solution was added dropwise to adjust the pH = 8.5–9.0. 20 mg $In_xSnO_2$ was added and continued stirring for 30 min. The mixed solution was heated at 130 °C in an oil bath for 4 h to ensure the complete reduction of Pt. During this process, a flow of $N_2$ kept passing through the solution to remove the dissolved oxygen. Then, the as-prepared sample was cooled to room temperature, washed with deionized water and centrifugated for several times. The precipitates were dried at 80 °C in a vacuum oven overnight. For all the samples, the Pt loading was kept at approximately 20 wt. %.

### 2.3. Physico-chemical characterizations of the samples

The morphology of the as-prepared samples was investigated using JEM-2100 transmission electron microscope (TEM) operating at 120 kV. X-ray diffraction (XRD) patterns were measured with a D8-Advance Bruker diffractometer at a scan rate of 4 deg/min ($30° < 2\theta < 85°$) and the wavelength of the incident radiation was 1.5406 Å (Cu K$\alpha$). X-ray photoelectron spectroscopy (XPS) measurements were taken on a Thermo ESCALAB 250 instrument with Al Ka radiation ($h$ = 1486.6 eV). The actual loading amount of Pt in the as-prepared catalysts was determined by inductively coupled plasma atomic emission spectrometry (ICP-AES, Perkin Elmer Optima-4300DV Spectrometer).

### 2.4. Electrochemical characterizations

A glassy carbon (GC) electrode of 5 mm diameter (surface area: 0.1963 $cm^2$) embedded in a Teflon holder was used as the working electrode. Prior to each use, the electrode was polished with 0.5 and 0.05 μm alumina suspensions followed by washed ultrasonically with $HNO_3$ (1:1), ethanol, acetone and deionized water, sequentially. The catalyst ink was prepared by sonicating a suspension of the $In_xSnO_2$-supported catalyst (5.0 mg) in isopropanol (1.0 mL). 10 μL of the suspension was firstly transferred onto the disk electrode, after the solvent evaporation at room temperature, 10 μL 0.05 wt. % Nafion solution (Dupont) was then pipetted onto the catalyst layer and air-dried. Since the actual Pt loading is slightly different for all of the catalysts, the MOR current normalized by the mass of Pt on the electrode was used for the comparison of the Pt catalytic activity in this study.

Electrochemical measurements were carried out on a CHI 660D (Shanghai Chenhua Apparatus, China). A conventional three-electrode cell was used for cyclic voltammetry (CV), CO-stripping and chronoamperometry (CA). A Pt foil (1.0 cm × 1.0 cm) and a

**Table 1**
XPS binding energies (eV) and surface compositions of the catalysts.

| Catalysts | Sn(IV) | | In(III) | | Pt(0) | | O1s | | Atomic O/Sn ratio |
|---|---|---|---|---|---|---|---|---|---|
| | $3d_{5/2}$ | $3d_{3/2}$ | $3d_{5/2}$ | $3d_{3/2}$ | $4f_{7/2}$ | $4f_{5/2}$ | Lattice oxygen | Adsorbed oxygen | |
| $Pt/In_{0.1}SnO_2$ | 486.9 | 495.3 | 444.8 | 452.3 | 71.2 | 74.5 | 530.7 | 532.2 | 2.04 |
| $Pt/In_{0.8}SnO_2$ | 487.0 | 495.4 | 445.3 | 452.8 | 71.2 | 74.5 | 530.8 | 532.2 | 3.03 |
| $Pt/SnO_2$ | 487.1 | 495.5 | | | 71.1 | 74.4 | 530.9 | 532.2 | 1.91 |
| Pure counterpart | 486.6 | 495.0 | 444.7 | 452.2 | 70.9 | 74.3 | | | |

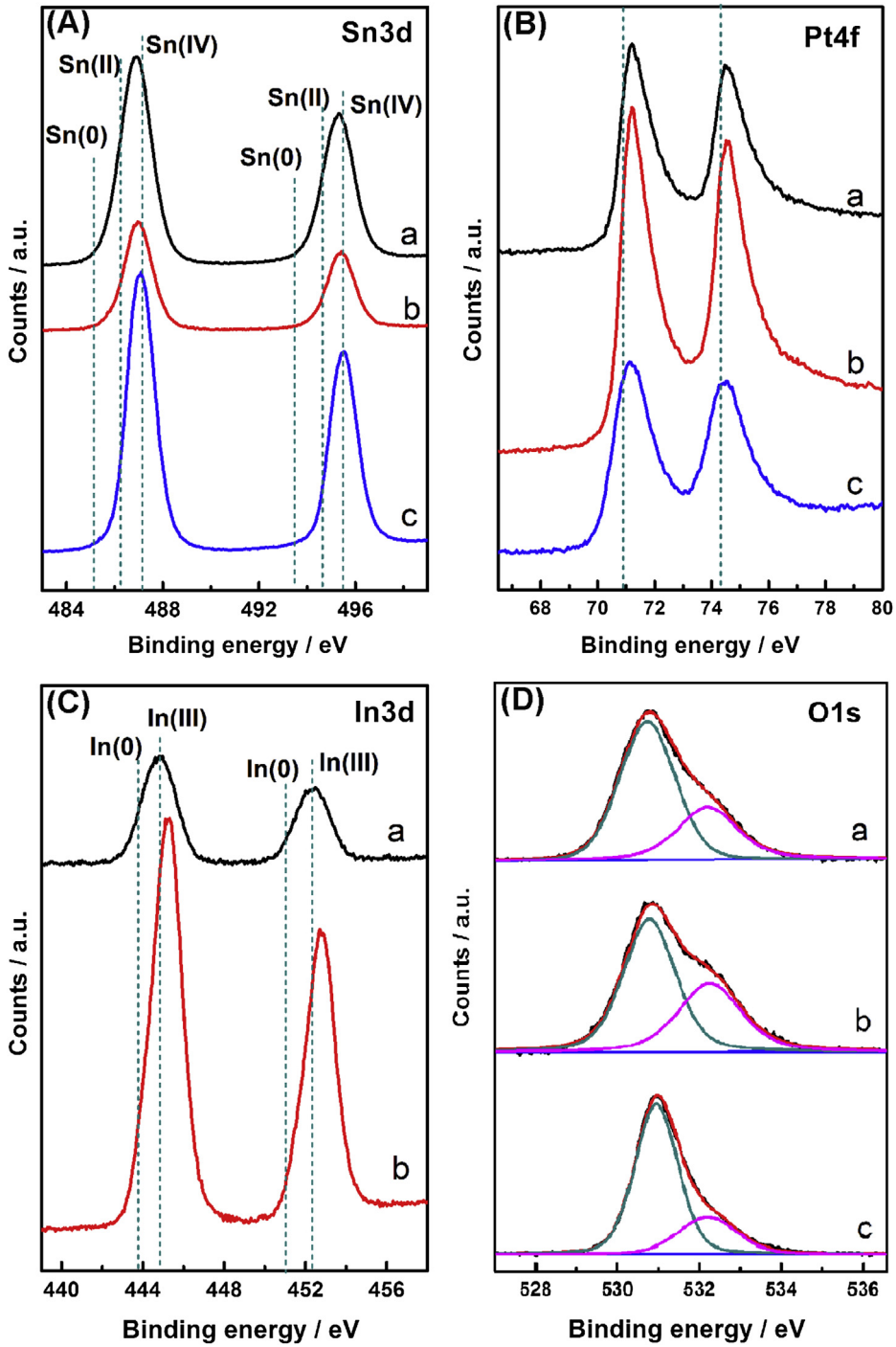


**Fig. 1.** (A) Sn3d, (B) Pt4f, (C) In3d and (D) O1s X-ray photoelectron spectra (XPS) of $Pt/In_{0.1}SnO_2$ (a), $Pt/In_{0.8}SnO_2$ (b) and $Pt/SnO_2$ (c) samples.

saturated calomel electrode (SCE) were used as the counter electrode and reference electrode, respectively. All potentials in this work are referred to the SCE. The electrolyte was 0.5 M KOH + 2.0 M $CH_3OH$ solution.

## 3. Results and discussion

### 3.1. Structural and morphology characterizations of the Pt/$In_xSnO_2$ samples

The chemical states of In, Sn, Pt and O elements and the surface compositions of the three as-prepared metal oxide supports are characterized by XPS (Fig. 1 and Table 1). The surface composition measurements show the atomic In/Sn ratio of the two In-doped $SnO_2$ supported samples is 0.1 and 0.8, which agrees well with that determined from EDS. The two In-doped $SnO_2$ supported Pt samples are therefore marked as Pt/$In_{0.1}SnO_2$ and Pt/$In_{0.8}SnO_2$, respectively. In Fig. 1, the vertical dotted lines in the figures refer to the binding energy (BE) positions for there "pure" counterparts. For Pt/$SnO_2$ sample, the BE positions of the symmetric peaks are around 487.1 and 495.5 eV for $Sn3d_{5/2}$ and $Sn3d_{3/2}$ (line c in Fig. 1A), respectively. For the other two In-doped $SnO_2$ supported Pt samples (line a and b in Fig. 1A), the Sn3d spectra are also symmetric and the BE positions show a slight shift to lower values. Compared with the positions of Sn(0), Sn(II) and Sn(IV) [29], the well-defined peaks of these In-doped $SnO_2$ supported Pt samples should be assigned to Sn(IV). Different from the signals of Sn3d, the BEs of Pt (Fig. 1B) of the three as-prepared samples shifted to higher values as compared with those of pure Pt/C sample [35], and the In-doped $SnO_2$ supported Pt samples (line a and b in Fig. 1B) showed more positive shifts as compared with that without In-doping (line c in Fig. 1B). The shifts of Pt are primarily a manifestation of electronic effects which induce changes in the Pt electronic structures. For Pt/$In_{0.1}SnO_2$ sample, the BEs of Pt4f spectra (Fig. 1B) shift to higher values and those of Sn3d spectra to lower values as compared with their "pure" counterparts, suggesting that the electronic interaction between Pt and $In_{0.1}SnO_2$ support may take a more active role in Pt/$In_{0.1}SnO_2$ than in other catalysts. The change in the work function of Pt may be responsible for the positive shift of Pt4f spectra [14]. The lower Pauling electronegativity of Sn(IV) than that of Pt would lead to a downshift of the Pt d-band center and consequently, a lower affinity of Pt for the adsorbates. This is crucial for the enhancement of the poison tolerance of Pt and the catalytic performance [13].

Besides the Sn3d and Pt4f signals, In3d peaks are also detected for the In-doped $SnO_2$ samples (Fig. 1C). Compared with the In(0) and In(III) positions, the symmetric peaks detected should correspond to the In(III). However, the specific compounds such as $In_2O_3$, $In(OH)_3$ or InOOH cannot be confirmed only from these XPS results, further analysis is shown in the next part. Both In and Sn elements in the composite metal oxides are in a high chemical state, suggesting the high stability of them during the cyclic voltammetry measurements. Since the In(III) XPS signals of Pt/$In_{0.1}SnO_2$ did not show significant shift as compared with the In(III) positions, therefore, the effect of In(III) on the electronic structure of Pt in Pt/$In_{0.1}SnO_2$ sample can be negligible, which is different from that of Sn3d spectra. Fig. 1D shows the O1s spectra of the three samples. By integrating the areas of O1s and Sn3d, it can be obtained that the atomic O/Sn ratio is about 3.0, 5.0 and 2.5 for Pt/$In_{0.1}SnO_2$, Pt/$In_{0.8}SnO_2$ and Pt/$SnO_2$ supported samples, respectively. These data are inconsistent with that of $SnO_2$ sample (atomic O/Sn ratio is 2.0), therefore, there should be other chemical states of O in the as-prepared supports. After being deconvoluted, the O1s peaks give us an interesting result. A semi-quantitative analysis, based on the integration areas of O1s peak at 530.8 eV, showed that the atomic O/Sn ratio is around 2.0 for Pt/$In_{0.1}SnO_2$ and Pt/$SnO_2$ supported samples. The specific data is 2.04 and 1.91, respectively, which is consistent with atomic O/Sn ratio of $SnO_2$. For Pt/$In_{0.8}SnO_2$ supported sample, the atomic O/Sn ratio is slightly larger (3.03), which may arise from the presence of In oxide in the support, specific analysis is shown in the next part. The peaks at low BE (ca. 530.8 eV) are assigned to the lattice oxygen of $SnO_2$, and the peaks at high BE (ca. 532.2 eV) should be attributed to the $H_2O$/OH adsorbed on the surfaces of $SnO_2$ or other metal oxides [36].

Fig. 2 shows the XRD patterns of the three supported Pt samples. The most three strongest diffraction peaks at 2$\theta$ positions 26.5°, 33.6°, 51.4°can be assigned to the crystal face of (110), (101) and (211) of $SnO_2$ (PDF # 41-1445), respectively. For Pt/$In_{0.1}SnO_2$ sample (Fig. 2a), except for the peaks belonging to Pt (marked with triangle) and $SnO_2$ (marked with dot), no signals corresponding to metallic phase of In or In oxides are detected, owing to the small amount of In in the sample or the amorphous state. For Pt/$In_{0.8}SnO_2$ sample (Fig. 2b), except for the significant diffraction peaks at the same 2$\theta$ positions with those of Pt/$In_{0.1}SnO_2$ and Pt/$SnO_2$ samples, several sharp peaks at 2$\theta$ positions 25.7°, 32.1°, 33.6° and 48.5° are detected, which can be assigned to the (110), (101), (011) and (211) crystal face of Indium oxide hydroxide (InOOH), respectively. (PDF # 17-0549). No peaks corresponding to metallic phase of In or other In oxides such as $In_2O_3$ and $In(OH)_3$ are detected. The average crystallite sizes of Pt in the three samples can be calculated from the (111) facet diffraction peaks using Scherrer's equation:

$$d = \frac{0.9\lambda_{k\alpha 1}}{B_{2\theta}\cos\theta_{\max}}$$

where $\lambda$ is the wavelength of the X-ray (1.54056 Å), $B_{2\theta}$ is the width of the peak at half-height, and $\theta$ is the angle at the maximum of the peak. The crystallite size of Pt in Pt/$In_{0.1}SnO_2$, Pt/$In_{0.8}SnO_2$ and Pt/$SnO_2$ samples is 2.8, 2.4 and 2.6 nm, respectively.

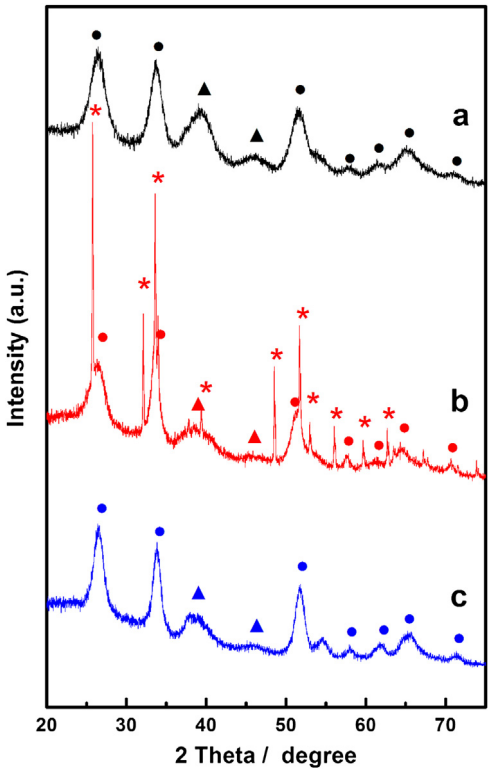


**Fig. 2.** XRD patterns of Pt/$In_{0.1}SnO_2$ (a), Pt/$In_{0.8}SnO_2$ (b) and Pt/$SnO_2$ (c) samples.

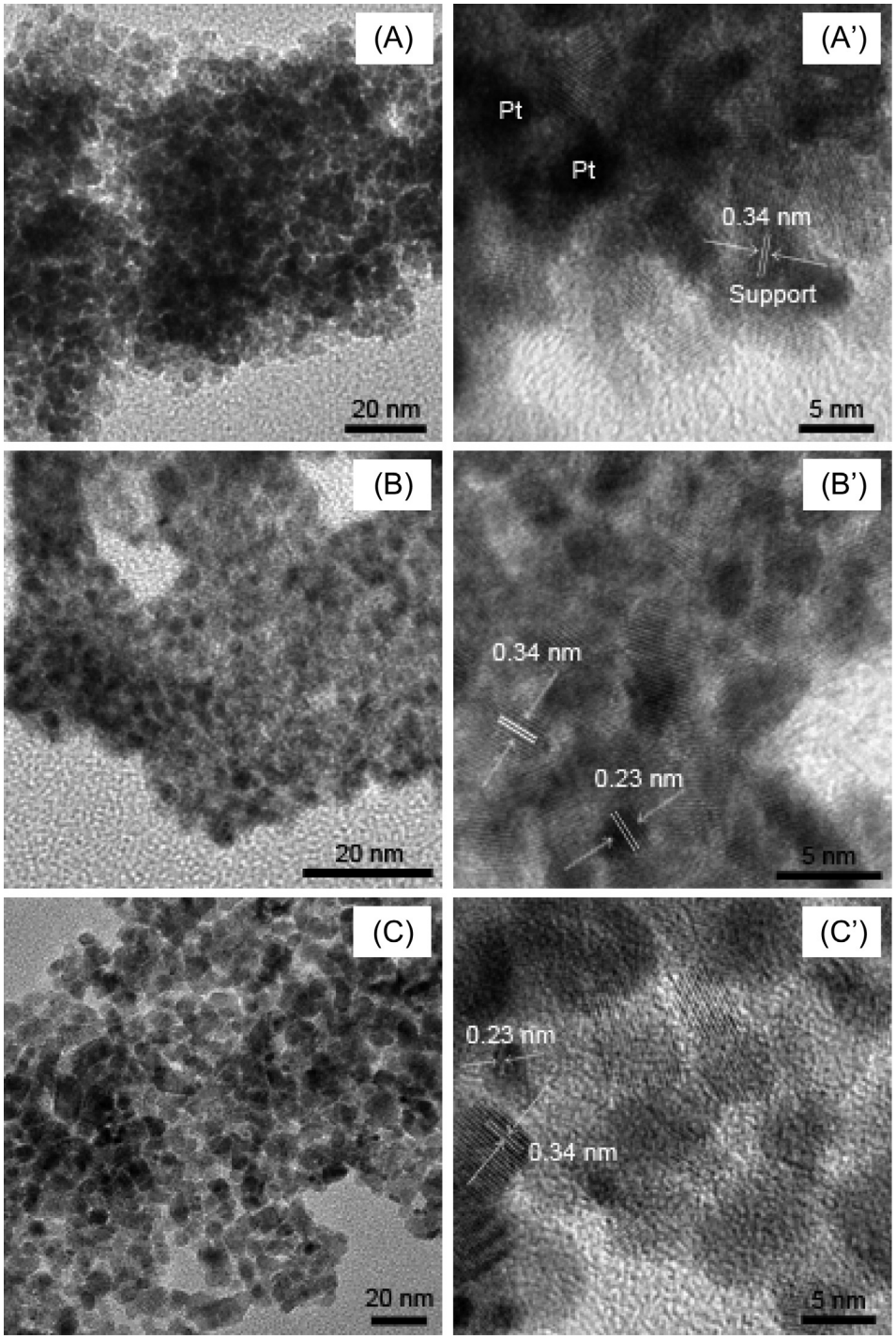


**Fig. 3.** TEM and HRTEM images of Pt/$In_{0.1}SnO_2$ (A and A′), Pt/$In_{0.8}SnO_2$ (B and B′) and Pt/$SnO_2$ (C and C′) samples. The fringe spacings of the support and Pt NPs are shown in the figures.

The representative morphologic features of the metal oxides supported Pt samples are shown in Fig. 3. All the support NPs exhibited a spherical-like shape, the mean particle sizes were evaluated from an ensemble of at least 200 particles in an arbitrarily chosen area of the corresponding TEM images. For $In_{0.1}SnO_2$, $In_{0.8}SnO_2$ and $SnO_2$ supports, the particle size was $5.2 \pm 0.8$, $2.9 \pm 0.4$ and $8.2 \pm 1.5$ nm, respectively. Although the particle sizes of the supports are very different, the sizes of Pt are almost the same and around 2.5 nm, as can be observed from the small darkly contrasting spherical Pt NPs dispersed on the supports. The sizes of Pt evaluated from TEM images agree well with those calculated from the XRD patterns. In addition, the crystallinity of all the supports is very apparent, the fringes of 0.34 nm corresponding to the spacing of (110) plane of $SnO_2$ are well-defined [37], which is in good agreement with the strongest diffraction signals in XRD patterns (Fig. 2). The fringes with lattice spacing of 0.23 nm are indexed as (111) of fcc Pt.

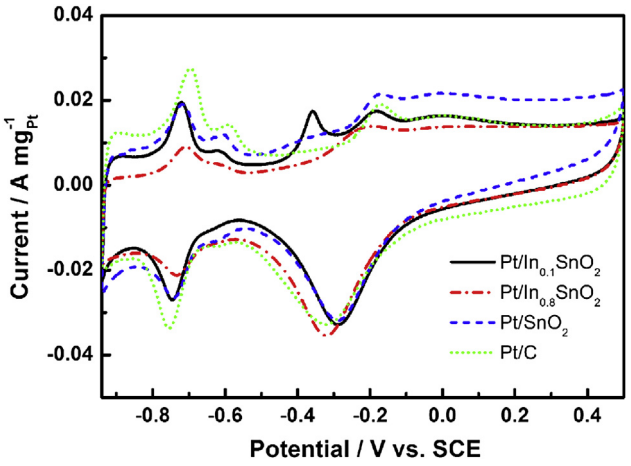


**Fig. 4.** Cyclic voltammograms of $Pt/In_{0.1}SnO_2$, $Pt/In_{0.8}SnO_2$, $Pt/SnO_2$ and commercial Pt/C catalysts in 0.5 M KOH (scan rate: 50 mV $s^{-1}$).

### 3.2. Cyclic voltammograms of $Pt/In_xSnO_2$ samples in alkaline electrolyte

Fig. 4 shows the cyclic voltammograms of the Pt catalysts supported on $In_xSnO_2$, $SnO_2$ and carbon black in 0.5 M KOH electrolyte without methanol. All the as-prepared samples showed similar CV features with Pt/C sample, suggesting that the metal oxides support did not show significant redox process in the tested potential range (−0.94 to 0.5 V). In the low potential side of the voltammograms, the cathodic/anodic peaks appearing between −0.94 and −0.5 V were assigned to the adsorption/desorption of atomic hydrogen on the Pt surface. These peaks corresponded to the typical signals of polycrystalline Pt, since the H adsorption/desorption processes are associated with the three low index crystal faces of Pt (110), (100) and (111). By integrating the coulombic charges associated with the hydrogen adsorption/desorption peaks, the electrochemically active surface area (EAS) of Pt in the three samples can be measured according to the following widely accepted equation [17,38]:

$$EAS = (Q_H/Q_e)A_{Pt}/W_{Pt}$$

This equation is established based on the well-accepted hydrogen-adsorption stoichiometry (H:Pt = 1:1) for polycrystalline Pt surface, where $Q_H$ is the charge consumed for the electro-oxidative desorption of adsorbed hydrogen from Pt, which is equivalent to the calibrated area of the hydrogen-desorption peaks (or anodic H peaks) that appear on the positive-going scan curve; $Q_e$ refers to the elementary charge (*i.e.*, the charge of an electron, $Q_e = 1.602 \times 10^{-19}$ C); $A_{Pt}$ is the area of an exposed Pt atom at the electrode, which is 0.077 $nm^2$ (obtained according to the atomic density for polycrystalline Pt surface: $1.3 \times 10^{15}$ $cm^{-2}$), and $W_{Pt}$ is the Pt loading by mass (weight in gram) at the working electrode. Thus:

$$EAS\ (m^2) = (Q_H/W_{Pt}) \times (A_{Pt}/Q_e) = Q_H/(0.21 \times W_{Pt})$$

The results of EAS are listed in Table 2. It is seen that the EAS data measured on $Pt/In_xSnO_2$ and $Pt/SnO_2$ are lower than that measured on the Pt/C sample, which may be due to the slight aggregation of Pt NPs on the metal oxide supports. For $Pt/In_{0.8}SnO_2$ sample, Pt shows the lowest EAS among the three as-prepared samples, suggesting the lowest dispersion state of Pt on the support. This phenomenon may arise from the too small size of the $In_{0.8}SnO_2$ support NPs (2.9 ± 0.4 nm), which is comparable to that of the carried Pt NPs (*ca.* 2.5 nm). In the high potential side of the voltammograms, the typical Pt-oxide region (>−0.30 V) was well-defined. A broad cathodic peak appeared at *ca.* −0.30 V can be assigned to the reduction of oxidized Pt. The shapes of the CV curves are consistent with those obtained by Sun and co-workers [39].

**Table 2**
Electrochemical parameters and activity for CO and methanol electro-oxidation on $Pt/In_{0.1}SnO_2$, $Pt/In_{0.8}SnO_2$, $Pt/SnO_2$ and commercial Pt/C catalysts.

| Catalysts | EAS[a] ($m^2$ $g^{-1}_{Pt}$) | $E_o$[b] (V) | $E_p$[c] (V) | $E_p$[d] (V) | MSA[e] (A $mg^{-1}_{Pt}$) | IA[f] (A $m^{-2}_{Pt}$) | Poisoning rate[g] |
|---|---|---|---|---|---|---|---|
| $Pt/In_{0.1}SnO_2$ | 43 | −0.72 | −0.30 | −0.24 | 2.32 | 54.4 | 0.0141 |
| $Pt/In_{0.8}SnO_2$ | 26 | −0.72 | −0.29 | −0.19 | 1.27 | 48.7 | 0.0154 |
| $Pt/SnO_2$ | 38 | −0.67 | −0.28 | −0.20 | 1.15 | 30.2 | 0.0201 |
| Pt/C (E-TEK) | 61 | −0.62 | −0.27 | −0.04 | 0.78 | 12.8 | 0.0158 |

[a] Electrochemically active surface area of Pt.
[b] Onset potential ($E_o$) for CO stripping.
[c] Peak potential ($E_p$) for CO stripping.
[d] Peak potential ($E_p$) for MOR.
[e] Mass specific activity at −0.24 V vs. SCE for MOR.
[f] Intrinsic activity at −0.24 V vs. SCE for MOR.
[g] Long-term poisoning rate of the catalysts calculated from the CA curves.

### 3.3. Methanol Electro-oxidation on $Pt/In_xSnO_2$ catalyst

The CV curves for MOR on the $Pt/In_xSnO_2$, $Pt/SnO_2$ and Pt/C catalysts in 0.5 M KOH electrolyte containing 2 M $CH_3OH$ are shown in Fig. 5. The currents of MOR are normalized to the mass of Pt on the electrode surface to give a rigorous comparison of the activity of Pt. It can be seen that all of the catalysts showed a well-defined anodic peak, which is related to the oxidation of methanol. All of the peak positions of the metal oxide supported Pt catalysts were more negative and the mass-specific activities (MSAs) of Pt were much higher than those of the commercial Pt/C catalyst. Among the

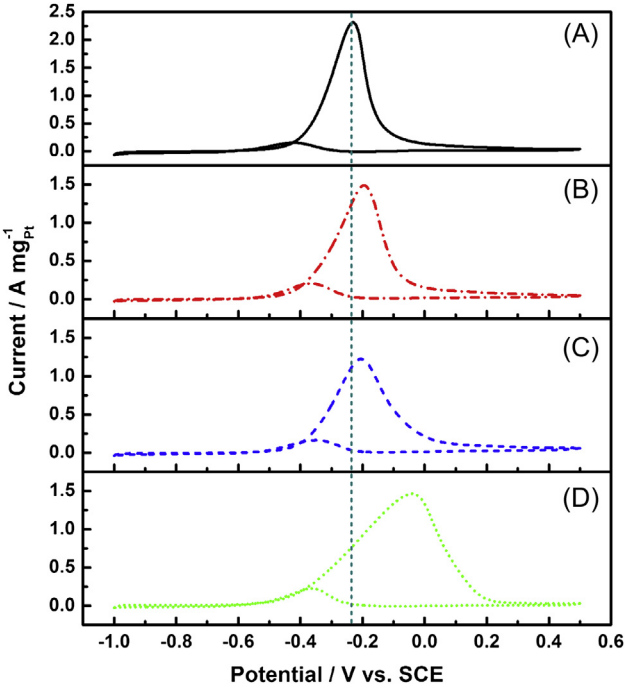


**Fig. 5.** Cyclic voltammograms of (A) $Pt/In_{0.1}SnO_2$, (B) $Pt/In_{0.8}SnO_2$, (C) $Pt/SnO_2$ and (D) Pt/C catalysts in 0.5 M KOH + 2.0 M $CH_3OH$ with the currents normalized to the mass of Pt on the surface of the electrode (scan rate: 20 mV $s^{-1}$).

as-prepared catalysts, $Pt/In_{0.1}SnO_2$ shows the most negative peak potential ($E_p$), the highest MSA and intrinsic activity (IA, IA = MSA/EAS). The number of $E_p$ (−0.24 V) for MOR was lowered by 40 and 200 mV, respectively, relative to those on the reference $Pt/SnO_2$ and Pt/C catalysts (see Table 2). The MSA data calculated at −0.24 V of $Pt/In_{0.1}SnO_2$, $Pt/In_{0.8}SnO_2$ and $Pt/SnO_2$ is 2.32, 1.27 and 1.15 A $mg^{-1}_{Pt}$, which is 3.0, 1.6 and 1.5 times that on the commercial Pt/C catalyst (0.78 A $mg^{-1}_{Pt}$), respectively. The above data indicated that the $SnO_2$ support could increase the catalytic activity of Pt as compared with the traditional carbon black support, and the introduction of In into the $SnO_2$ support could significantly further improve the catalytic activity of Pt toward MOR. In addition, it is interesting that the catalytic activity of Pt was strongly dependent on the composition of the support. Introduction of a small amount of In in the support ($In_{0.1}SnO_2$) proves to be advantageous to the promoting effect to Pt whereas large content of In in the support ($In_{0.8}SnO_2$) seems not so good. The difference in the electronic structure of Pt in the catalysts may contribute to the enhancement in the activity of Pt, as can be confirmed by the XPS results (Fig. 1). For the metal oxide supported Pt samples, the BEs of Pt4f shifted to higher values as compared with pure Pt sample. Meanwhile, the Sn3d signals in $In_xSnO_2$ samples shifted to lower values as compared with pure $SnO_2$ supported Pt catalysts. These phenomena suggest that there is electronic interaction between Pt and the $In_xSnO_2$ supports, which modified the surface electronic structure of Pt, i.e. downshift of the d-band center of the Pt, and thus resulted in a weakened interaction between Pt and the adsorbed intermediate species [13]. This may be the root reason of the enhancement in Pt catalytic activity toward MOR. For the two $In_xSnO_2$ supported catalysts, besides the difference in the BEs of Sn3d, the BEs of In3d in $Pt/In_{0.1}SnO_2$ sample (444.8 and 452.3 eV) exhibited lower values by 0.5 eV as compared those in $Pt/In_{0.8}SnO_2$ sample (445.3 and 452.8 eV), which may be another factor affecting the catalytic properties of Pt in the two $Pt/In_xSnO_2$ samples. Large content of InOOH in the support did not show further promoting effect to Pt catalysis probably arising from the inappropriate modification of the electronic structure of Pt.

The CO stripping voltammograms of the metal oxide supported Pt and commercial Pt/C samples are shown in Fig. 6. Different from the simple profile of CO oxidation on Pt catalyst in acidic electrolyte [40], three anodic peaks in the positive-going scans during the CO oxidation were observed on all of the catalysts. Take $Pt/In_{0.1}SnO_2$ catalyst for an example, the voltammogram of CO oxidation first exhibits fast current-rising with the onset potential ($E_o$) at around −0.75 V, then a current plateau region from −0.60 to −0.48 V followed by fast current-rising again. After the second current plateau from −0.38 to −0.35 V the current showed a dramatic increase until a current peak is seen at −0.30 V. This phenomenon is similar with the result reported by Jiang and coworkers [41]. The complexity of the oxidation profile could be due to the formation of formate intermediate during the CO electrooxidation process in alkaline electrolyte. CO is likely to react with bulk $OH^-$ to give soluble formate via the following equation: $CO + OH^-(aq) \rightarrow HCOO^-(aq)$, the soluble formate is more facile to be electro-oxidized than CO through the following equation: $HCOO^-(aq) + OH^-(aq) \rightarrow CO_2 + H_2O + 2e^-$. In addition, it is reported that the profile of CO electro-oxidation was dependent on the potential sweep rate [42]. E. Santos et al. reported that the oxidation current peaks would shift towards more positive values and the three oxidation peaks gradually overlapped to give a single broad asymmetric peak with increasing the sweep rate. The $E_o$ and $E_p$ for CO oxidation on the catalysts are given in Table 2. Though both the numbers of $E_o$ and $E_p$ were different from each other for the $In_xSnO_2$ supported Pt catalysts, they were consistently lower than those on the reference catalyst with carbon black as the support. For $Pt/In_{0.1}SnO_2$ catalyst, both the $E_o$ and $E_p$ exhibit the most negative values among the catalysts, suggesting that a small amount of In doping in $SnO_2$ could significantly enhance the CO tolerance of Pt and exhibit high promoting effect to the Pt catalysis.

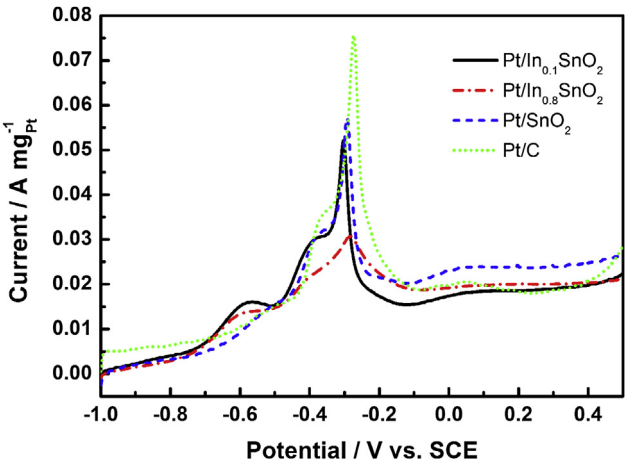


**Fig. 6.** CO stripping voltammograms of $Pt/In_{0.1}SnO_2$, $Pt/In_{0.8}SnO_2$, $Pt/SnO_2$ and commercial Pt/C catalysts in 0.5 M KOH + 2.0 M $CH_3OH$.

In view of the above CV results, the main reaction pathway of MOR can be explained by bifunctional mechanism [2,15,43,44]. Specific processes are given as follows:

$$CH_3OH + 4OH^- \rightarrow CO_{ad} + 4H_2O + 4e^- \quad (1)$$

Methanol is firstly oxidized to adsorbed CO intermediate on the Pt surface, the adsorbed CO is subsequently oxidized to $HCOO^-$ at a relatively high potential [41]:

$$CO_{ad} + OH^-(aq) \rightarrow HCOO^-(aq) \quad (2)$$

At a more positive potential (>−0.35 V), the adsorbed $HCOO^-$ is oxidized to $CO_2$ by the $OH^-$ (aq), as described below:

$$HCOO^-(aq) + OH^-(aq) \rightarrow CO_2 + H_2O + 2e^- \quad (3)$$

Besides the $OH^-$ in the solution, the adsorbed $OH_{ads}$ on the surface of $In_{0.1}SnO_2$ can also oxidize the neighboring intermediates adsorbed on the Pt surface through the following equations [44]:

$$In_{0.1}SnO_2 + OH^- \rightarrow In_{0.1}SnO_2 - OH_{ads} + e^- \quad (4)$$

$$In_{0.1}SnO_2 - OH_{ads} + Pt - CO_{ads} + OH^- \rightarrow In_{0.1}SnO_2 + Pt + CO_2 + H_2O + e^- \quad (5)$$

A standard test of MOR catalyst tolerance to CO poisoning during continuous fuel cell operation is based on the assessment of their medium term activity under constant potential conditions [45]. Fig. 7 shows the chronoamperometry (CA) behaviors of the $Pt/In_xSnO_2$ and Pt/C catalysts at −0.4 V for 3600 s. All of the catalysts featured a pronounced current decay in the first 10 min, which could arise from the accumulation of poisonous intermediates [46], then the current decay slowed down at longer times. For $In_{0.1}SnO_2$ catalyst, both the initial and limiting methanol oxidation currents are relatively higher than the other catalysts, showing a higher electrocatalytic activity for MOR. This result is consistent with that of the CV results shown in Fig. 5. The long-term poisoning rates ($\delta$) for the catalysts were calculated by measuring the linear decay of the current at times greater than 1500 s from Fig. 7 according the following equation [47,48]:

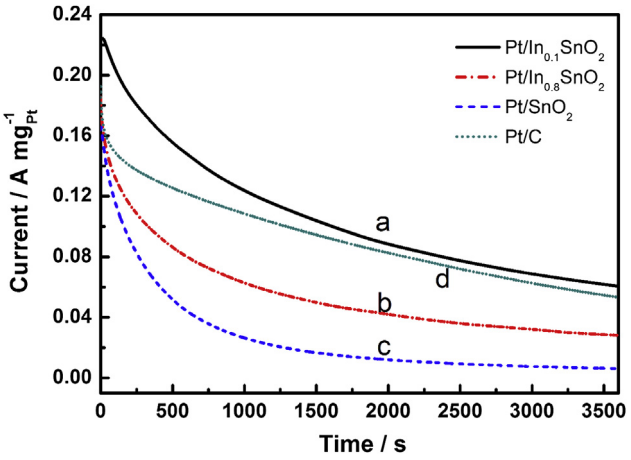


**Fig. 7.** Chronoamperograms of $Pt/In_{0.1}SnO_2$, $Pt/In_{0.8}SnO_2$, $Pt/SnO_2$ and commercial Pt/C catalysts in 0.5 M KOH + 2.0 M $CH_3OH$ at −0.4 V.

$$\delta = \frac{100}{I_0} \times \left(\frac{dI}{dt}\right)_{t>1500\ s}$$

where $(dI/dt)_{t>1500\ s}$ is the slope of the linear portion of the current decay and $I_0$ is the current at the start of polarization back extrapolated from the linear current decay. The calculated data of $\delta$ are listed in Table 2. $Pt/In_{0.1}SnO_2$ catalyst not only maintained a higher level overall methanol oxidation current than the other catalysts but also exhibited the lowest long-term poisoning rate, suggesting that a small amount of In doping in $SnO_2$ support showed a high promoting effect to Pt catalytic activity and stability toward MOR. This can be attributed to the change in the electronic structure of Pt as discussed in the preceding sections.

## 4. Conclusions

This work developed a kind of non-carbon composite metal oxide supports that demonstrated higher catalytic activity toward methanol electrooxidation reaction as compared with the commercial Pt/C catalyst. The improvement was strongly dependent on the composition of the supports. Among the catalysts, $Pt/In_{0.1}SnO_2$ exhibited the lowest peak potential, the highest MSA and IA, suggesting that a small amount of In doping in $SnO_2$ was advantageous to the Pt catalysis. XPS results confirmed that composite metal oxide supports $In_xSnO_2$ could lead to the changes in the electronic structure of Pt, the downshift of the d-band center was responsible for the enhancement of the catalytic activity of Pt. The above findings derived from our study not only would be informative for understanding the role of electronic structure of Pt in determining the electrocatalysis toward MOR in alkaline electrolyte, but also would be promising in designing new catalysts that can replace the traditional catalytic nanostructure.

## Acknowledgments

This work is supported by Scientific Research Foundation for the Outstanding Young Scientist of Shandong Province (BS2011NJ009), Natural Science Foundation of Shandong Province (ZR2010EM026) and National Innovation and Entrepreneurship Training Program for Undergraduates (201310446015).

## References

[1] E. Antolini, E.R. Gonzalez, J. Power Sources 195 (2010) 3431.
[2] J.S. Spendelow, A. Wieckowski, Phys. Chem. Phys. Chem. 9 (2007) 2654.
[3] M. Bergelin, E. Herrero, J.M. Feliu, M. Wasberg, J. Electroanal. Chem. 467 (1999) 74.
[4] L.X. Ding, A.L. Wang, G.R. Li, Z.Q. Liu, W.X. Zhao, C.Y. Su, Y.X. Tong, J. Am. Chem. Soc. 134 (2012) 5730.
[5] K.S. Lee, I.S. Park, H.Y. Park, T.Y. Jeon, Y.E. Sung, Catal. Today 146 (2009) 20.
[6] J. Luo, P.N. Njoki, Y. Lin, D. Mott, L.Y. Wang, C.J. Zhong, Langmuir 22 (2006) 2892.
[7] Y.Y. Feng, L.X. Bi, Z.H. Liu, D.S. Kong, Z.Y. Yu, J. Catal. 290 (2012) 18.
[8] S. Papadimitriou, S. Armyanov, E. Valova, A. Hubin, O. Steenhaut, E. Pavlidou, G. Kokkinidis, S. Papadimitriou, J. Phys. Chem. C 114 (2010) 5217.
[9] A. Tegoua, S. Papadimitrioua, I. Mintsoulia, S. Armyanovb, E. Valovab, G. Kokkinidisa, S. Sotiropoulos, Catal. Today 170 (2011) 126.
[10] J. Zhang, M.B. Vukmirovic, Y. Xu, M. Mavrikakis, R.R. Adzic, Angew. Chem. Int. Ed. 44 (2005) 2132.
[11] J.R. Kitchin, J.K. Nørskov, M.A. Barteau, J.G. Chen, J. Chem. Phys. 120 (2004) 10240.
[12] A. Ruban, B. Hammer, P. Stoltze, H.L. Skriver, J.K. Nørskov, J. Mol. Catal. A 115 (1997) 421.
[13] M. Wakisaka, S. Mitsui, Y. Hirose, K. Kawashima, H. Uchida, M. Watanabe, J. Phys. Chem. B 110 (2006) 23489.
[14] M. Weinert, R.E. Watson, Phys. Rev. B 51 (1995) 17168.
[15] T. Frelink, W. Visscher, A.P. Cox, J.A.R. van Veen, Electrochim. Acta 40 (1995) 1537.
[16] J.S. Wang, J.Y. Xi, Y.X. Bai, Y. Shen, J. Sun, L.Q. Chen, W.T. Zhu, X.P. Qiu, J. Power Sources 164 (2007) 555.
[17] P. Justin, G.R. Rao, Catal. Today 141 (2009) 138.
[18] P.K. Shen, C.W. Xu, R. Zeng, Y.L. Liu, Electrochem. Solid-State Lett. 9 (2006) A39.
[19] C.W. Xu, P.K. Shen, Chem. Commun. (2004) 2238.
[20] C.W. Xu, P.K. Shen, Y.L. Liu, J. Power Sources 164 (2007) 527.
[21] C.W. Xu, R. Zeng, P.K. Shen, Z.D. Wei, Electrochim. Acta 51 (2005) 1031.
[22] E. Auer, A. Freund, J. Pietsch, T. Tacke, Appl. Catal. A 173 (1998) 259.
[23] S.Y. Huang, P. Ganesan, S. Park, B.N. Popov, J. Am. Chem. Soc. 131 (2009) 13898.
[24] S. Takenaka, H. Matsumori, K. Nakagawa, H. Matsune, E. Tanabe, M. Kishida, J. Phys. Chem. C 111 (2007) 15133.
[25] Z.Z. Jiang, Z.B. Wang, W.L. Qu, D.M. Gu, G.P. Yin, Appl. Catal. B 123–124 (2012) 214.
[26] D.A. Konopka, M. Li, K. Artyushkova, N. Marinkovic, K. Sasaki, R. Adzic, T.L. Ward, P. Atanassov, J. Phys. Chem. C 115 (2011) 3043.
[27] V.T.T. Ho, C.J. Pan, J. Rick, W.N. Su, B.J. Hwang, J. Am. Chem. Soc. 133 (2011) 11716.
[28] C.V. Subban, Q. Zhou, A. Hu, T.E. Moylan, F.T. Wagner, F.J. DiSalvo, J. Am. Chem. Soc. 132 (2010) 17531.
[29] W.P. Zhou, S. Axnanda, M.G. White, R.R. Adzic, J. Hrbek, J. Phys. Chem. C 115 (2011) 16467.
[30] H.T. Lu, Y. Fan, P. Huang, D.L. Xu, J. Power Sources 215 (2012) 48.
[31] D.B. Yu, D.B. Wang, W.C. Yu, Y.T. Qian, Mater. Lett. 58 (2004) 84.
[32] J. Liu, C. Zhong, X.T. Du, Y.T. Wu, P.Z. Xu, J.B. Liu, W.B. Hu, Electrochim. Acta 100 (2013) 164.
[33] I.S. Park, E. Lee, A. Manthiram, J. Electrochem. Soc. 157 (2010) B251.
[34] W.X. Du, Q. Wang, D. Saxner, N.A. Deskins, D. Su, J.E. Krzanowski, A.I. Frenkel, X.W. Teng, J. Am. Chem. Soc. 133 (2011) 15172.
[35] E.A. Ashok, P. Kundu, P.A. Deshpande, G. Madras, N. Ravishankar, ACS Nano 5 (2011) 8049.
[36] P. Stefanov, G. Atanasova, E. Manolov, Z. Raicheva, V. Lazarova, J. Phys. Conf. Ser. 100 (2008) 082046.
[37] J.F. Ye, H.J. Zhang, R. Yang, X.G. Li, L.M. Qi, Small 6 (2010) 296.
[38] D. Zhao, B.Q. Xu, Angew. Chem. Int. Ed. 45 (2006) 4955.
[39] M.Y. Jing, L.H. Jiang, B.L. Yi, G.Q. Sun, J. Electroanal. Chem. 688 (2013) 172.
[40] A. Pozio, M. De Francesco, A. Cemmi, F. Cardellini, L. Giorgi, J. Power Sources 105 (2002) 13.
[41] J. Jiang, A. Wieckowski, Electrochem. Commun. 20 (2012) 121.
[42] E. Santos, M.C. Giordano, J. Electroanal. Chem. 172 (1984) 201.
[43] J.H. Ma, Y.Y. Feng, J. Yu, D. Zhao, A.J. Wang, B.Q. Xu, J. Catal. 275 (2010) 34.
[44] A.V.P. Palenzuela, E. Brillas, C. Arias, F. Centellas, J.A. Garrido, R.M. Rodríguez, P.L. Cabot, J. Catal. 298 (2013) 112.
[45] H.A. Gasteiger, N. Markovi, P.N. Ross Jr., E.J. Cairns, J. Phys. Chem. 97 (1993) 12020.
[46] A. Kabbabi, R. Faure, R. Durand, B. Beden, F. Hahn, J.M. Leger, C. Lamy, J. Electroanal. Chem. 444 (1998) 41.
[47] J. Jiang, A. Kucernak, J. Electroanal. Chem. 543 (2003) 187.
[48] J.W. Guo, T.S. Zhao, J. Prabhuram, R. Chen, C.W. Wong, Electrochim. Acta 51 (2005) 754.